LANGMUIR Article
Cite This: Langmuir 2019, 35, 10808−10817
pubs.acs.org/Langmuir

Modeling Lower Critical Solution Temperature Behavior of Associating Dendrimers Using Density Functional Theory

Yuchong Zhang and Walter G. Chapman*

Department of Chemical and Biomolecular Engineering, Rice University, 6100 Main Street, Houston, Texas 77005, United States

ABSTRACT: We study the phase behavior of associating dendrimers in explicit solvents using classical density functional theory. The existence of association enables uptake of solvent inside the dendrimer even for unfavorable Lennard-Jones interaction between the solvent and dendrimer. Depending on the distributions of associating sites, the dendrimer conformation can be either dense-core or dense-shell. The conformation of the associating dendrimer is greatly affected by the temperature. Due to the interplay between association interaction and Lennard-Jones attractions, we find the lower critical solution temperature (LCST) behavior of dendrimer conformation and study how it changes as the dendrimer size or solvent size changes. The dendrimer in our study displays no LCST behavior at low generations, and it has a maximum LCST at *G*4. Moreover, increasing the solvent chain length decreases the LCST. For solvents with self-association, the competition between solvent-solvent association and solvent-dendrimer association also tends to reduce the LCST. Qualitatively consistent with experiments, our results provide insight into the molecular mechanism of the LCST behavior of associating dendrimers.

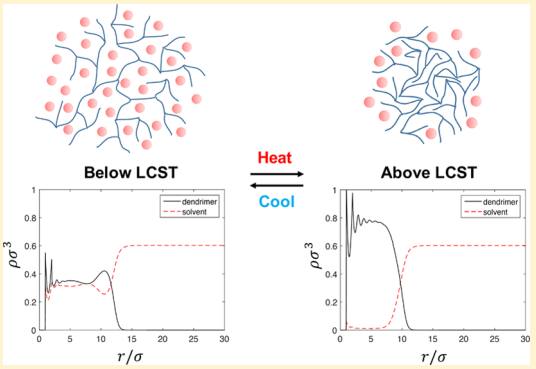

INTRODUCTION

Thermoresponsive polymers[1,2] show sharp and reversible changes in conformations and properties near the lower critical solution temperature (LCST). In aqueous solution, these polymers hydrate and expand below the LCST while collapse and form aggregates above the LCST. Polyethylene glycol (PEG)[2] and poly(*N*-isopropylacrylamide) (PNIPAM)[3] are the most often investigated thermoresponsive linear polymers. Nowadays, there is considerable interest in designing thermoresponsive dendritic polymers.[4−19] Dendritic polymers, unlike linear polymers, are highly branched, and therefore, they have a specific spheroid-like shape and multifunctionality. Among all dendritic polymers, dendrimers are perfectly branched and well-defined. With the advantage of structural uniformity, thermoresponsive dendrimers are highly attractive for promising applications, such as drug delivery.[20,21]

One of the first works for thermoresponsive dendrimers was carried out by Haba et al.,[4] where they introduced isobutyramide (IBAM) groups to the chain ends of poly(amidoamine) (PAMAM) or poly(propyleneimine) (PPI) and successfully produced dendrimers with temperature-sensitive water solubility. They further found that LCSTs of IBAM-bearing PAMAM dendrimers varied with different generation numbers, pH, and concentrations. By modifying the terminal segments with functional groups such as phenylalanine residues,[5] Tono et al. successfully synthesized thermosensitive dendrimers that were more suitable for use in biomedical fields. Later, Haba et al.[7] compared the thermosensitve properties of PAMAM dendrimers with peripheral *N*-isopropylamide groups and linear polymers with the same functional groups and found that although they both featured LCST, there was a marked difference in the transition enthalpy between the linear molecule and dendrimer molecule. Liu et al.[8] compared the LCST behavior of polyethylenimine (modified with IBAM)-based dendrimers, hyperbranched polymers, and linear polymers and found that LCSTs of dendrimers were not as sensitive to the molecular weight alteration as hyperbranched polymer analogues but more sensitive than linear analogues.

Instead of modifying terminal segments, Parrott et al.[14] encapsulated the hydrophobic carborane functionality within the interior of the dendrimer and also imparted the LCST behavior to an otherwise fully water-soluble structure. Xu et al.[15] synthesized H40-poly(*N*-isopropylacrylamide)-poly(2-(dimethylamino)ethyl methacrylate) (H40-PNIPAM-PDMA), which exhibited two-stage collapse because PNIPAM and PDMA have different LCSTs.

These studies, in preparing thermoresponsive denderimers, generally fall into two different strategies. One is the incorporation of temperature-responsive groups onto dendrimers,[15,19] and the other is the grafting of both hydrophobic and hydrophilic functionalities.[4,5,7−9,14] The spirits of two strategies are the same in that the temperature sensitivity is induced as a result of competing interactions. While the temperature-responsive groups have both favorable and unfavorable interactions with the solvent, the second strategy works as well with the appropriate balance of hydrophilic and hydrophobic moieties.

Received: February 20, 2019
Revised: July 17, 2019
Published: July 23, 2019

DOI: 10.1021/acs.langmuir.9b00514
Langmuir 2019, 35, 10808−10817

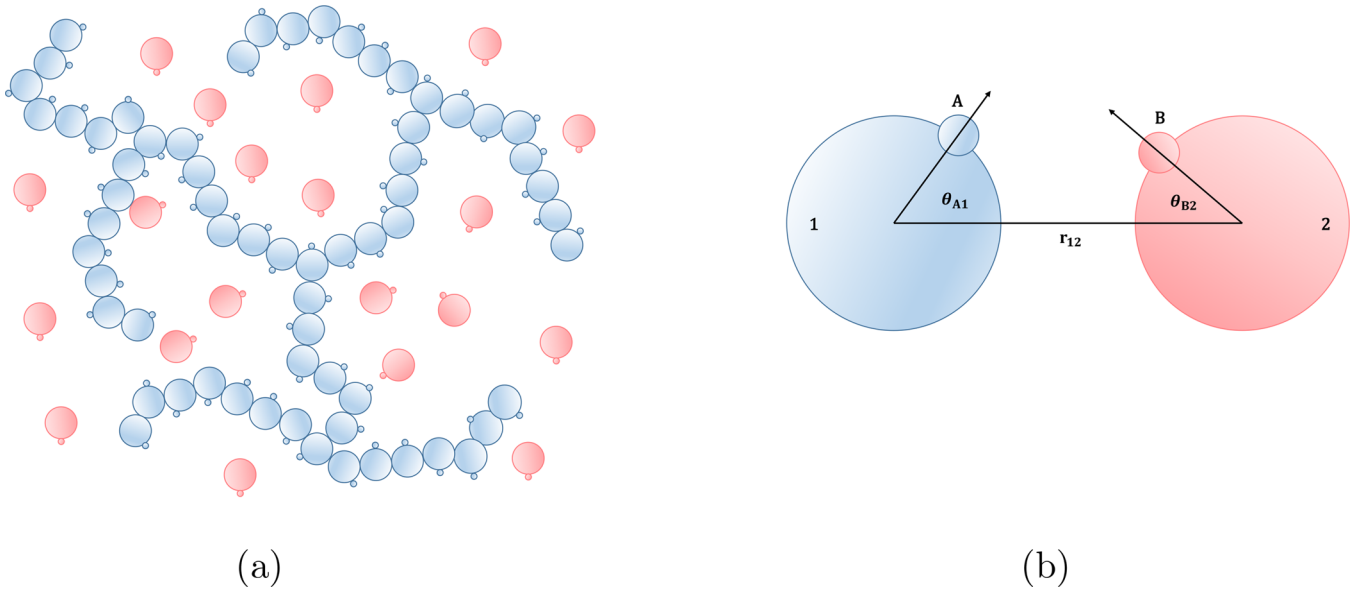

Figure 1. (a) Schematic of a dendrimer (blue) with a single associating site at each segment. The solvent (pink) is spherical with a single associating site. (b) Schematic of association interaction.

In terms of applications, Li et al.[20] found that the PAMAM dendrimers modified with alkoxy diethylene glycol not only showed sharply changed surface properties between hydrophilic and hydrophobic at approximate human body temperature but also had much lower cytotoxicity than that of their parent PAMAM dendrimers, making them a promising material to construct intelligent drug delivery systems. Kimura et al.[17] studied the catalysis activity for a temperature-sensitive dendritic host. The catalysis ability increased above the LCST because the incorporated catalyst was accessible to substrates after the dendrimer shrank, and in this way, the reaction was controlled by the temperature.

Apart from the experimental design and property characterization of thermoresponsive dendrimers, there are also theoretical or simulation works for modeling of dendrimers[22−27] or thermoresponsive polymers (and polymer brushes).[28−31] However, few of them are directly devoted to the study of thermoresponsive dendrimers. This work begins to fill this gap and brings insights into the molecular mechanism of thermoresponsive dendrimers. In our previous work, we have used inhomogeneous statistical associating fluid theory (iSAFT) to study the conformation of an isolated dendrimer in solvents of varying quality and found that the solvent size, density, chemical affinity, and temperature all play a role in determining a solvent to be good or poor.[32] Those theoretical results reached semiquantitative agreement with molecular simulation. As a density functional theory (DFT)[33−36] for inhomogeneous complex polymeric fluids, iSAFT is based on rigorous statistical mechanics[37−40] and proved to provide detailed fluid structures at a fraction of the calculation expense of molecular simulation methods.[41,42] Meanwhile, iSAFT is able to describe fluids with association, such as hydrogen bonding, which we believe is of the utmost importance in explaining thermoresponsive behavior of dendrimers. The association sites can be modeled at specific positions of the molecule and explicit bonding are expected within the association range. Therefore, in this work, we use iSAFT to model associating dendrimers, and the paper is organized as follows. In Theory, we explain the system of interest and the iSAFT theory. In Results and Discussion, we first explore the hydrogen bond effect on associating dendrimers and then dive into the LCST behavior. Within a vast parameter space, we focus on understanding how dendrimer generation, solvent size, and association model would impact the phase behavior. Conclusions gives our conclusion.

THEORY

Interaction Potential Model. The system of interest is depicted in Figure 1a. A single dendrimer is immersed into explicit solvents, and the core of the dendrimer is fixed as the origin. The dendrimer molecule is modeled as a flexible chain of tangentially bonded spherical segments. The functionality of branched segments is set as 3, and the spacer between the branched segments is set as 7. While the dendrimer of generation 1 ($G1$) in Figure 1a is already quite large, its size will increase exponentially as the generation increases. Solvent molecules are modeled as spheres or linear chains of spheres, which may have favorable or unfavorable interactions with the dendrimer. All the segments in the system are treated to have a temperature-independent hard sphere diameter σ, and they interact through pairwise repulsive, attractive, and association contributions, given by the following pair potential

$$u(\mathbf{r}_{12}, \omega_1, \omega_2) = u^{\mathrm{ref}}(\mathbf{r}_{12}) + u^{\mathrm{att}}(r_{12}) + \sum_{\mathrm{A}}\sum_{\mathrm{B}} u_{\mathrm{AB}}^{\mathrm{assoc}}(\mathbf{r}_{12}, \omega_1, \omega_2) \quad (1)$$

where r_{12} is the distance between two segments and ω_1, ω_2 are the orientations of segments 1 and 2, respectively.

The reference fluid contribution u^{ref} is often taken as a hard sphere repulsive interaction

$$u^{\mathrm{ref}}(\mathbf{r}_{12}) = u^{\mathrm{hs}}(r_{12}) = \begin{cases} \infty, & r_{12} < \sigma \\ 0, & r_{12} \geq \sigma \end{cases} \quad (2)$$

The intermolecular attractions u^{att} are described as a cut-shifted Lennard-Jones (LJ) attraction with a Weeks, Chandler, and Andersen (WCA) separation,[43,44]

DOI: 10.1021/acs.langmuir.9b00514
Langmuir 2019, 35, 10808−10817

$$u^{\mathrm{att}}(r_{12}) = \begin{cases} u^{\mathrm{LJ}}(r_{\mathrm{min}}) - u^{\mathrm{LJ}}(r_c) & \text{if } \sigma < r_{12} \le r_{\mathrm{min}} \\ u^{\mathrm{LJ}}(r_{12}) - u^{\mathrm{LJ}}(r_c) & \text{if } r_{\mathrm{min}} < r_{12} \le r_c \end{cases} \quad (3)$$

where

$$u^{\mathrm{LJ}}(r_{12}) = 4\varepsilon^{\mathrm{LJ}}\left[\left(\frac{\sigma}{r_{12}}\right)^{12} - \left(\frac{\sigma}{r_{12}}\right)^{6}\right] \quad (4)$$

$r_{\mathrm{min}} = 2^{1/6}\sigma$ is the position of the Lennard-Jones potential minimum and $r_c = 2.5\ \sigma$ is the cutoff distance. The sum of u^{ref} and u^{att} serves as an approximation of the cut and shifted Lennard-Jones potential.

Finally, the association potential is given by

$$u_{\mathrm{AB}}^{\mathrm{assoc}}(\mathbf{r}_{12}, \omega_1, \omega_2) = \begin{cases} -\varepsilon_{\mathrm{AB}}^{\mathrm{assoc}}, & r_{12} < r_c;\ \theta_{\mathrm{A1}} < \theta_c;\ \theta_{\mathrm{B2}} < \theta_c \\ 0, & \text{otherwise} \end{cases} \quad (5)$$

where θ_{A1} is the angle between the vector from the center of segment 1 to site A and vector $\mathbf{r}_{12}$ and θ_{B2} is the angle between the vector from the center of segment 2 to site B and the vector $\mathbf{r}_{12}$, as shown in Figure 1b. The radial limits of square-well association are set to $r_c = 1.05\sigma$ and the angular limit to $\theta_c = 27°$.

iSAFT Density Functional Theory. Traditional iSAFT DFTs are formulated for an open system in the grand canonical ensemble. Therefore, the system is at a fixed volume (V), temperature (T), and chemical potential (μ) in the presence of an external field ($V^{\mathrm{ext}}(\mathbf{r})$). The grand free energy functional $\Omega[\rho]$ for a system of chain fluids can be related to the intrinsic Helmholtz free energy functional $A[\rho]$ as

$$\Omega[\rho_i(\mathbf{r})] = A[\rho_i(\mathbf{r})] - \sum_{i=1}^{m}\int \mathrm{d}\mathbf{r}'\rho_i(\mathbf{r}')(\mu_i - V_i^{\mathrm{ext}}(\mathbf{r}')) \quad (6)$$

where ρ_i is the density of segment i, μ_i is its chemical potential, V_i^{ext} is the external field acting on segment i, and the sum is over all the m segments in the system. For the system at equilibrium, the grand free energy is minimized. Minimization of the grand free energy with respect to the density of the segments yields a system of variational equations, known as the Euler−Lagrange equations,

$$\frac{\delta A[\rho_i(\mathbf{r})]}{\delta\rho_i(\mathbf{r})} = \mu_i - V_i^{\mathrm{ext}}(\mathbf{r}),\ \forall\ i = 1, \ldots, m \quad (7)$$

The contribution due to the Helmholtz free energy functional can be decomposed into an ideal and excess contribution.

$$A[\rho_i(\mathbf{r})] = A^{\mathrm{id}}[\rho_i(\mathbf{r})] + A^{\mathrm{ex,hs}}[\rho_i(\mathbf{r})] + A^{\mathrm{ex,chain}}[\rho_i(\mathbf{r})] + A^{\mathrm{ex,att}}[\rho_i(\mathbf{r})] + A^{\mathrm{ex,assoc}}[\rho_i(\mathbf{r})] \quad (8)$$

The ideal contribution comes from the ideal gas state of the atomic mixture (id). The excess contribution of the free energy is due to hard sphere excluded volume effects (hs), chain connectivity (chain), long-range attraction (att), and association (assoc). For conciseness, the formulation for each term is given in Appendix.

However, the system in our study is different from the traditional iSAFT DFT since the number of dendrimer segments is fixed. Therefore, it is more accurate to name such a system as a semicanonical ensemble where V, T, M_{D} (number of dendrimer segments), and μ_{S} (chemical potential of solvent) are fixed. In this semicanonical ensemble, the equilibrium density profile of the polymer and solvent is obtained by minimizing the semicanonical free energy functional

$$A'[\rho_i(\mathbf{r})] = A[\rho_i(\mathbf{r})] + \sum_i \int \mathrm{d}\mathbf{r}\rho_i(\mathbf{r})V_i^{\mathrm{ext}}(\mathbf{r}) - \int \mathrm{d}\mathbf{r}\rho_S(\mathbf{r})\mu_S \quad (9)$$

Note that we will use D and S as subscripts to represent the properties for the dendrimer or solvent. The constraint on the number of dendrimer segments is given by

$$\int \mathrm{d}\mathbf{r}\rho_D(\mathbf{r}) = M_D \quad (10)$$

By using the Lagrange multiplier technique, we construct the free energy functional as

$$A[\rho_i(\mathbf{r})] + \sum_i \int \mathrm{d}\mathbf{r}\rho_i(\mathbf{r})V_i^{\mathrm{ext}}(\mathbf{r}) - \int \mathrm{d}\mathbf{r}\rho_S(\mathbf{r})\mu_S - \mu_D\left[\int \mathrm{d}\mathbf{r}\rho_D(\mathbf{r}) - M_D\right] \quad (11)$$

where μ_D is the "chemical potential" of the dendron (the branch that originates from the central core) imposed by the tether condition that there are three such dendrons.

By minimizing the above functional with respect to ρ_i, we can obtain

$$\frac{\delta A[\rho_i(\mathbf{r})]}{\delta\rho_D(\mathbf{r})} + V_D^{\mathrm{ext}}(\mathbf{r}) - \mu_D = 0 \quad (12)$$

$$\frac{\delta A[\rho_i(\mathbf{r})]}{\delta\rho_S(\mathbf{r})} + V_S^{\mathrm{ext}}(\mathbf{r}) - \mu_S = 0 \quad (13)$$

There are three equations (eqs 10, 12, 13) with three unknown variables ρ_D, ρ_S, and μ_D. To obtain the density profiles of each component, we solve these equations simultaneously. The numerical algorithm is the same as in our previous paper.[32] Note that, in the previous paper, the position variable in equations 27−45 should be in the vector form $\mathbf{r}$ instead of the scalar form r, which is a typo. Due to the spherical symmetry of the dendrimer structure, all segment densities are only functions of radial distance from the center core, and we are able to solve these equations in only one dimension.

RESULTS AND DISCUSSION

Effect of Hydrogen Bonding on Dendrimer Structure. To model the effect of hydrogen bonding on dendrimer structure, we first adopt the basic association scheme: each dendrimer or solvent segment has one association site, and it is limited to bond at most once; association is only possible between a dendrimer segment and solvent segment (see Figure 1a). For simplicity, we set $\varepsilon_{DD}^{\mathrm{LJ}}/k_{\mathrm{b}} = \varepsilon_{SS}^{\mathrm{LJ}}/k_{\mathrm{b}} = 150$ K, $\varepsilon_{DS}^{\mathrm{LJ}}/k_{\mathrm{b}} = 0$, and $\varepsilon_{DS}^{\mathrm{assoc}}/k_{\mathrm{b}} = 2700$ K. Note that the energy parameter is coupled with the Boltzmann constant k_{b} so its unit is in Kelvin. The LJ energy parameters are chosen to mimic a poor solvent condition for the dendrimer molecule. The association energy is similar in magnitude to energies used to model association of alcohols. Although simple, this setup is able to model the

DOI: 10.1021/acs.langmuir.9b00514
Langmuir 2019, 35, 10808−10817

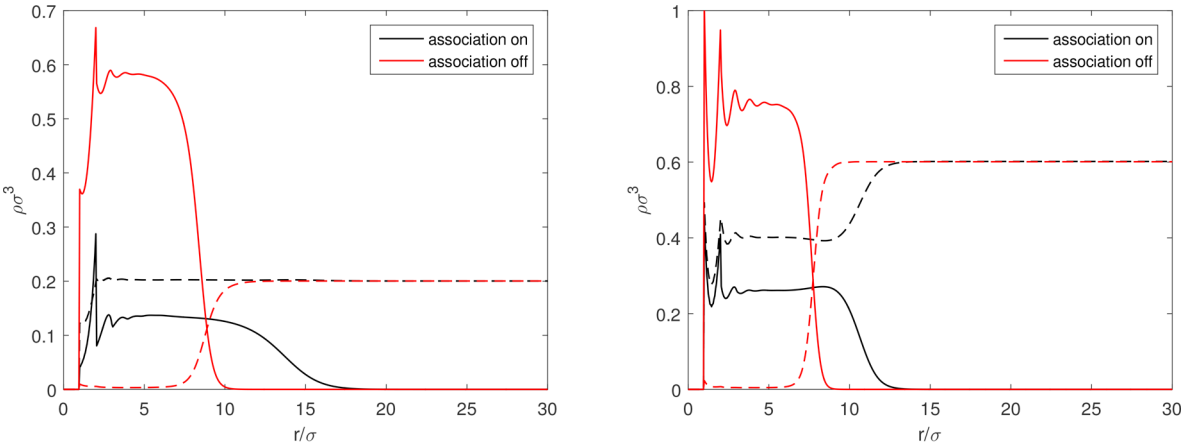

Figure 2. Density profiles of G5 dendrimer in spherical solvents at T = 300 K. $\varepsilon^{LJ}_{DD}/k_b = \varepsilon^{LJ}_{SS}/k_b$ = 150 K, $\varepsilon^{LJ}_{DS}/k_b$ = 0. $\varepsilon^{assoc}_{DS}/k_b$ = 2700 K when association is on, and $\varepsilon^{assoc}_{DS}/k_b$ = 0 when association is off. Solid curves represent dendrimer monomers, and dashed curves represent solvents. (a) $\rho_S\sigma^3$ = 0.2 at bulk. (b) $\rho_S\sigma^3$ = 0.6 at bulk.

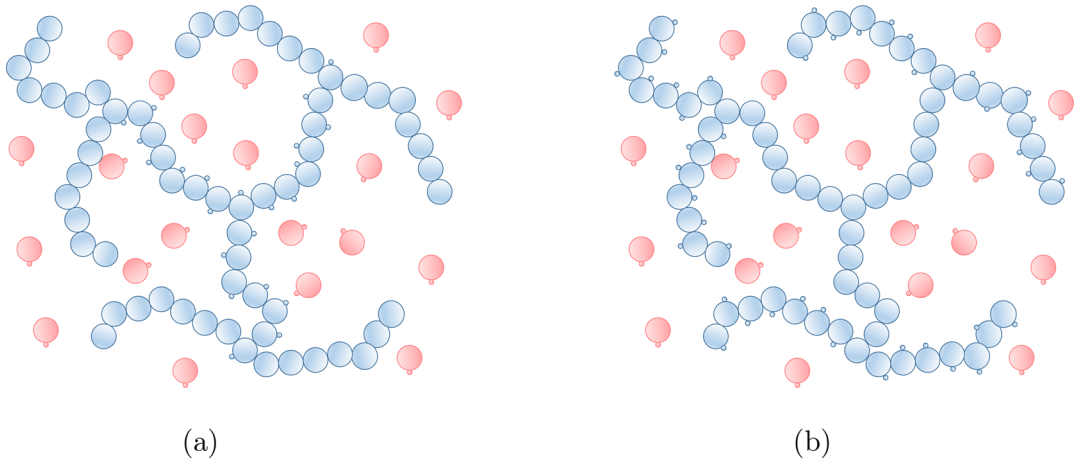

Figure 3. (a) Schematic of a dendrimer (blue) with a single associating site at each inner segment. (b) Schematic of a dendrimer (blue) with a single associating site at each outer segment. For both cases, the solvent (pink) has a single associating site.

balance between hydrogen bonding and van der Waals interactions. As shown in Figure 2, at T = 300 K, the dendrimer G5 collapses when there is no association and expands with the association on for both low ($\rho_S\sigma^3$ = 0.2, corresponding to a dense gas) and high ($\rho_S\sigma^3$ = 0.6, corresponding to a liquid) solvent densities. This significant change demonstrates that the existence of hydrogen bonding is likely to change the quality of solvent, and in this example, association between dendrimer and solvent results in a good solvent. Similar behaviors are observed from experiments of Chai et al.[45] where they found that DAB (poly(propylene imine)) would swell in chloroform solutions but collapse in benzene.

Instead of having one association site at each dendrimer segment, it is possible to design a nonuniform distribution of association sites. Particularly, it is of experimenters' interest to understand how different layouts of functional groups would impact the material properties. Therefore, we also study the case where only the inner segments (excluding the segments of outermost shell) have an associating site per segment (the inner-sites model, see Figure 3a) and the case where only the outer segments (segments of outermost shell) have an associating site per segment (the outer-sites model, see Figure 3b). While the outer-sites model have more associating sites than the inner-sites model, the margin is relatively small compared to the total numbers of sites when the generation number is high. For reference, we name the dendrimer in Figure 1a as full-sites model. From Figure 4, we see that, at 300 K, these three different G5 dendrimers (full-sites, inner-sites, and outer-sites) show quite different conformations with the same parameters. Only the full-sites dendrimer displays a fully extended conformation because it has nearly twice the number of associating sites compared with the other two dendrimers. What we also find is that the inner-sites dendrimer forms a dense-shell structure and the outer-sites dendrimer forms a dense-core structure. The association of dendrimer monomers with solvents reduces the monomer density, but this effect is constrained by the locality of associating sites. Therefore, we see two different structures for different layouts of associating sites. The controversy of a dendrimer being a dense-shell structure or dense-core structure has been around for decades, and it is agreed that the answer varies case by case, depending on the design of dendrimer and also the solvent.[24,25,27,46−49] While most past studies are focused on amphiphilic

DOI: 10.1021/acs.langmuir.9b00514
Langmuir 2019, 35, 10808−10817

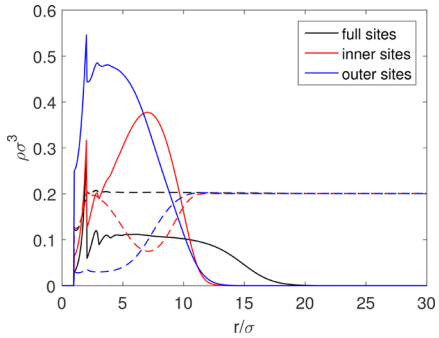

Figure 4. Density profiles of *G*5 dendrimer (full-sites, inner-sites, and outer-sites) in associating spherical solvents at different temperatures. $\varepsilon^{LJ}_{DD}/k_b = \varepsilon^{LJ}_{SS}/k_b = 150$ K, $\varepsilon^{LJ}_{DS}/k_b = 0$, $\varepsilon^{assoc}_{DS}/k_b = 2700$ K, and $\rho_S\sigma^3 = 0.2$ at bulk. Solid curves represent dendrimer monomers, and dashed curves represent solvents.

dendrimers,[25,27,48] this study shows that, by imparting association at different regions of dendrimer, it is also possible to observe these two different structures. In addition, for the inner-sites dendrimer to form a dense-shell structure, it is not necessary to have a segregation effect between the inner and outer monomers as required in some amphiphilic dendrimer studies,[25,27] though introduction of such a segregation effect may further contribute to the formation of a dense-shell structure.

In our previous DFT study, we found that, if we only consider dispersion, a higher temperature always improves the solvent quality regardless of the affinity between the dendrimer and solvent.[32] Here, in Figure 5, we show how temperature

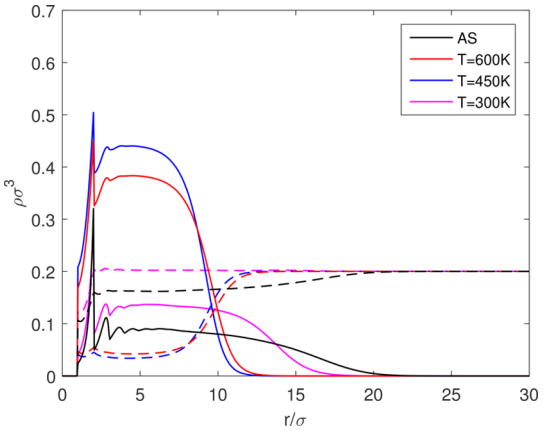

Figure 5. Density profiles of *G*5 dendrimer in associating spherical solvents at different temperatures. $\varepsilon^{LJ}_{DD}/k_b = \varepsilon^{LJ}_{SS}/k_b = 150$ K, $\varepsilon^{LJ}_{DS}/k_b = 0$, $\varepsilon^{assoc}_{DS}/k_b = 2700$ K, and $\rho_S\sigma^3 = 0.2$ at bulk. Solid curves represent dendrimer monomers, and dashed curves represent solvents.

affects the system when dispersion and association both exist. We use the full-sites *G*5 dendrimer, and it is found that the dendrimer collapses when the temperature is raised from 300K to 450K and becomes less compressed at $T = 600$ K. As the temperature goes to infinity, which is the athermal (AS) condition, a fully swollen structure is recovered. This finding is fascinating since it indicates that presence of multiple interactions might cause a complex phase behavior.[13,50,51] The temperature dependence of this model system can be likened to a dendrimer solution that features both the lower critical solution temperature (LCST) and the upper critical solution temperature (UCST) with a closed-loop. That is, the solution is miscible for all compositions at low and high temperatures but is prone to phase separation at intermediate temperatures. Unlike the LCST behavior, no UCST behavior of dendrimers has been reported yet from the literature. It is possible that the dendrimer would decompose before the transition occurs despite that UCST exists theoretically . Therefore, we focus on the LCST behavior of dendrimers for the following sections and stick with the full-sites model for the upcoming results and discussions.

LCST of Associating Dendrimers. Even the lower critical solution temperature is not that easy to find. LCST is generally believed to be a first-order transition, and normally a discontinuity or a sharp change in solubility-related properties as the temperature varies would be an indicator of LCST transition, such as the transmittance of solution. We experiment with different combinations of parameters and end up with the following parameter values in search of LCST: $\varepsilon^{LJ}_{DD}/k_b = \varepsilon^{LJ}_{SS}/k_b = 250$ K, $\varepsilon^{LJ}_{DS}/k_b = 0$, and $\varepsilon^{assoc}_{DS}/k_b = 2700$ K. In addition, the bulk solvent density is fixed at 0.6.

For a full-sites *G*6 dendrimer in this type of system, we find that at $T = 282$ K, the dendrimer is relatively swollen, and there is a substantial amount of solvent inside the interior of dendrimer (Figure 6a). However, as temperature increases to $T = 286$ K, we see a dramatic change in the conformation of the dendrimer as the dendrimer collapses. Also, the solvent is depleted in the dendrimer (Figure 6b).

The collapse of the dendrimer is due to the LJ attraction between dendrimer segments combined with the unfavorable LJ interaction between dendrimer and solvent segments. When the temperature is low, the association between the dendrimer and solvent works as a counter force and contributes to the solvation of the dendrimer. At a higher temperature, the association between the dendrimer and solvent weakens, and the LJ interaction becomes the dominant factor that makes the dendrimer collapse.

In the interior region of a swollen dendrimer, as we can see from Figure 6c, a substantial amount of dendrimer and solvent segments are bonded. In this case, the association interaction dominates the system, and the solvents can easily penetrate inside the dendrimer. By comparison, Figure 6d shows that, at $T = 286$ K, association only occurs in a very narrow range at the periphery of the dendrimer. Figure 6e,f shows the schematics of dendrimer structures at low and high temperatures, respectively.

To quantify the structure of dendrimer, we calculate the radius of gyration R_g from

$$R_g^2 = \frac{\int \rho_D(r) r^4 \mathrm{d}r}{\int \rho_D(r) r^2 \mathrm{d}r} \tag{14}$$

For the transition region, we first start at a lower temperature with a swollen structure, gradually increasing the temperature and getting a series of swollen structures until the dendrimer collapses. We then start at a higher temperature with a collapsed dendrimer structure, gradually decreasing the temperature and getting a series of collapsed structures until the dendrimer swells. Figure 7 shows the radius of gyration for all these structures. At several temperatures, there are both swollen and collapsed structures so there forms a hysteresis loop. The hysteresis loop is a result of the calculation scheme of density functional theory, which uses Picard iteration for convergence. At a certain condition, the Picard iteration stops

DOI: 10.1021/acs.langmuir.9b00514
Langmuir 2019, 35, 10808−10817

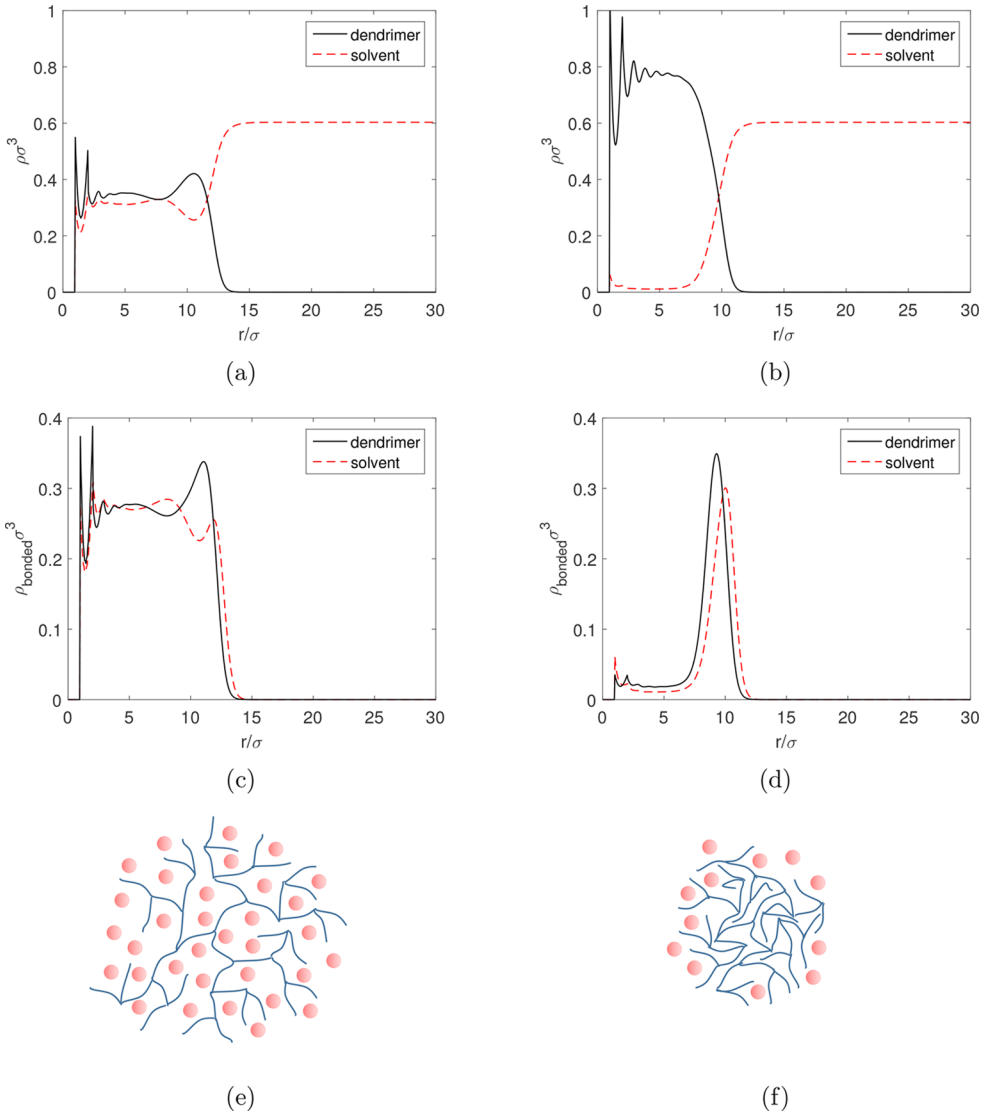

Figure 6. Results for a full-sites *G6* dendrimer in an associating solvent. (a) Density profiles of *G6* dendrimer and solvent segments at T = 282 K. (b) Density profiles of *G6* dendrimer and solvent segments at T = 286 K. (c) Density profiles of bonded dendrimer and solvent segments at T = 282 K. (d) Density profiles of bonded dendrimer and solvent segments at T = 286 K. (e) Schematic of swollen dendrimer with solvents. (f) Schematic of collapsed dendrimer with solvents. Other parameters are fixed: $\varepsilon_{DD}^{LJ}/k_b = \varepsilon_{SS}^{LJ}/k_b$ = 250 K, $\varepsilon_{DS}^{LJ}/k_b$ = 0, $\varepsilon_{DS}^{assoc}/k_b$ = 2700 K, and $\rho_S\sigma^3$ = 0.6 at bulk.

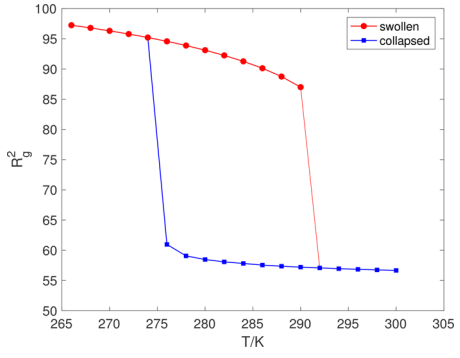

Figure 7. R_g^2 hysteresis of the *G6* dendrimer in associating spherical solvents.

when the difference of the last two iterations is within the error tolerance. Just like in molecular simulation where the system might be stuck in the metastable state (local minimum) if there is not enough energy disturbance, the converged result in DFT can also be a metastable state if the step size (mixing of the old and new iterations) is not big enough. To figure out which structure is actually the stable one at a specific temperature and pinpoint the exact transition temperature, we calculate the free energy for each state. The semicanonical free energy difference for two structures versus temperature is plotted in Figure 8. At temperatures lower than 284 K, the swollen structure has a lower free energy than the collapsed structure and is the stable one. At temperatures higher than 284 K, the free energy of collapsed structure is lower, so the dendrimer would collapse. Therefore, for this system, LCST is around 284 K. Without using any empirical temperature-dependent parameter, our theory successfully captures the LCST behavior of hydrogen bonding dendrimers. We can also calculate the size change for the dendrimer molecule based on the radius of gyration and find that the dendrimer in our model shrinks by 26.5% from the swollen state at 282 K to the collapsed state at 286 K. This shrinkage is comparable to the experimental study of Li et al.[20]

DOI: 10.1021/acs.langmuir.9b00514
Langmuir 2019, 35, 10808−10817

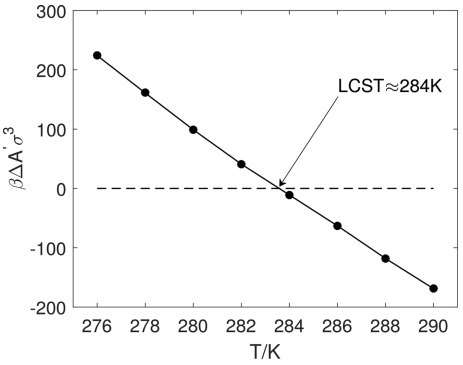

Figure 8. Difference in semicanonical free energy between the swollen and collapsed structures ($\Delta A' = A'_{collapsed} - A'_{swollen}$) versus temperatures for the *G*6 associating dendrimer.

where the size of PAMAM dendrimer shrank by about 35% around the LCST.

We further study how the generation number of dendrimer in our model would affect the LCST. For dendrimers *G*0 to *G*3, there is no apparent LCST transition behavior. This is consistent with the study of Haba et al.[4] (LCST starts from *G*3), Aathimanikandan et al.[13] (LCST starts from *G*1), and Parrott et al.[52] (LCST starts from *G*3), where no LCST was observed for lower generations. However, the trends on how LCST changes for higher generations are all different from these experiments. While Haba et al. found that LCST decreases as the generation grows, in the study of Parrott et al., LCST of dendrimers showed a nonmonotonic change with different generations. In our model, the LCST of *G*4 is 306 K, and for both *G*5 and *G*6, the LCST is 284 K (see Figure 9a). This trend is similar to the finding of Aathimanikandan et al., where they found that LCST decreases significantly from *G*1 to *G*2 and stays almost constant in *G*3. Also, there is actually more similarity between the dendron design (they studied a thermoresponsive dendron instead of a dendrimer) of Aathimanikandan et al. and our model than the other two experimental studies. In the study of Aathimanikandan et al., LCST was brought about by the incorporation of oligoethylene glycol units in both interior and terminal regions; therefore, the dendrimer design corresponds to our full-sites model. The dependence of LCST on generation was a result of the combination of these amphiphlic moieties and dendritic effect. Therefore, a possible explanation for the trend observed in our model is the following. The dendrimer is more open at lower generations so that there is more contact between internal association sites and solvents. The dendrimer becomes denser, and its surface begins to close upon itself with increasing generation; as a result, the solvents mainly interact with the terminal association site and the LCST drops. After certain generations, the favorable association and unfavorable LJ interaction reach a balance and result in a plateauing LCST.

Instead of changing the dendrimer size by changing the generation number, we can also model how the LCST varies when the solvent size changes, such as the chain length of a linear solvent. To keep the same amount of bonding sites, each segment of the solvent has a single associating site that can interact with the dendrimer. From Figure 9b, we see that when the solvent chain length increases, LCST decreases. This trend can be accounted by the entropic effect of the solvents of different sizes. As the solvent molecule gets larger, there must be more favorable energetic gain for the dendrimer to swell, leading to a lower LCST.

Self-association of Solvent. In this section, we consider the case that solvent molecules have self-association. We previously considered only solvent-dendrimer association. Here, we study how the competition between solvent-solvent association versus solvent-dendrimer association affects the LCST. The limit of zero solvent-solvent association energy produces the results shown in Figure 9.

Solvent-solvent association is often the case in real systems, and the dendrimer model developed in this work is easily extended to different association schemes. For example, a water molecule is often modeled with either two, three, or four association sites with two different types of association sites A and B, representing hydrogen or oxygen sites. Site A can associate with site B. For our system, we consider a two-sites solvent molecule with one site A and one site B. Site A can also associate with site C on the dendrimer. However, no association occurs between site B and site C. While keeping all the other parameters the same as in previous cases, we vary the self-association energy parameter ϵ_{AB}^{assoc} between site A and site B and see how that affects the phase behavior of the dendrimer at different temperatures.

From Figure 10, we see that for dendrimer of *G*5, as the self-association strength ϵ_{AB}^{assoc} increases but still lower than ϵ_{AC}^{assoc}, LCST decreases. This is because of the competition between site B of solvent and site C of dendrimer in associating with site A of solvent. Figure 11 shows the bonded density profile

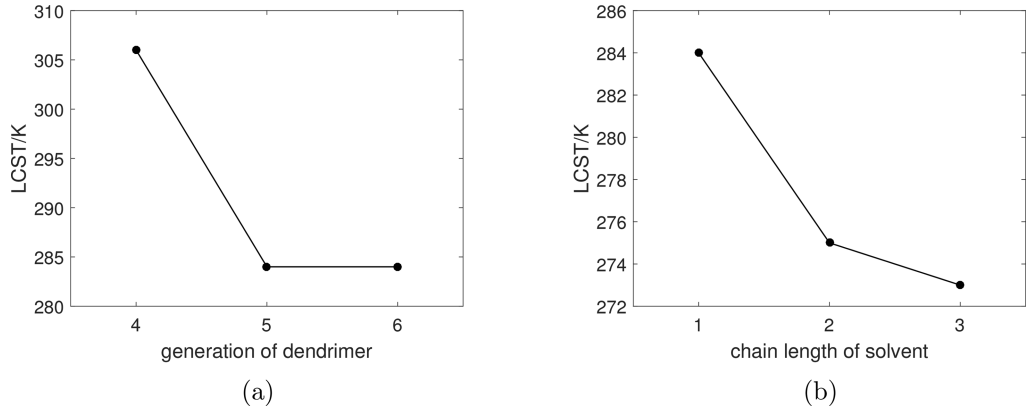

Figure 9. (a) LCST as a function of dendrimer generation number. Solvent is spherical. (b) LCST as a function of solvent length. The dendrimer is for *G*5. Other parameters are the same as Figure 8.

DOI: 10.1021/acs.langmuir.9b00514
Langmuir 2019, 35, 10808−10817

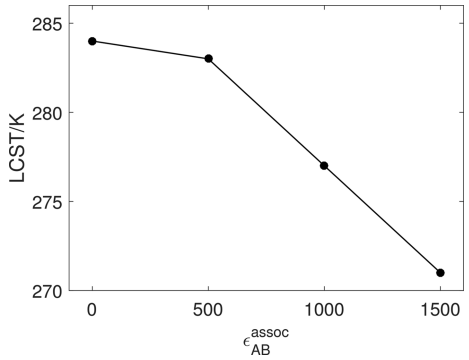

Figure 10. LCST of *G*5 dendrimer for spherical solvents of different self-association energy ε^{assoc}_{AB}. $\varepsilon^{LJ}_{DD}/k_b = \varepsilon^{LJ}_{SS}/k_b = 250$ K, $\varepsilon^{LJ}_{DS}/k_b = 0$, $\varepsilon^{assoc}_{AC}/k_b = 2700$ K, and $\rho_S\sigma^3 = 0.6$ at bulk.

for those sites at different temperatures. The dendrimer is swollen at 275 K and collapsed at 280 K. Since $\varepsilon^{assoc}_{AB} < \varepsilon^{assoc}_{AC}$, site B is less active where dendrimer segments exist, but the introduction of competition tends to drive LCST to the lower temperature. Actually, when we further increase ε^{assoc}_{AB} beyond ε^{assoc}_{AC}, the dendrimer would be highly collapsed at all temperatures, the solvents are completely depleted from the dendrimer, and no LCST behavior is observed.

CONCLUSIONS

Understanding the effect of association, such as hydrogen bonding, on the conformation of dendrimers is of great importance for thermoresponsive material design. In this study, we have applied iSAFT to study the structure of a single dendrimer in explicit solvents and found that the inclusion of association will lead to interesting phase behaviors that are not observed if only dispersion is considered. The solubility of dendrimer in solvents can be tuned by the association and dispersion strength, and both dense-core and dense-shell conformations of dendrimers can form depending on the molecular design. We have also captured the LCST behavior of associating dendrimers at high generations and explored the parameters (i.e., solvent size, self-association of solvent) that can affect the phase behavior. LCST is found to decrease as the solvent size increases or the self-association strength of solvent increases. These results demonstrate iSAFT's capability to model the hydrogen bonding effect of dendrimer systems and provide guidance in the design and synthesis of real materials.

APPENDIX

Free Energy Functional

Here, we list the analytical forms for the different free energy contributions in eq 8.

The ideal gas functional is known exactly as

$$\beta A^{id}[\rho_i(\mathbf{r})] = \int d\mathbf{r}_1 \sum_{i=1}^{m} \rho_i(\mathbf{r}_1)[\ln \rho_i(\mathbf{r}_1) - 1] \tag{15}$$

The hard sphere contribution $A^{ex,\,hs}[\rho_i(\mathbf{r})]$ is calculated from Rosenfeld's fundamental measure theory (FMT)[53] for a mixture of hard spheres:

$$\beta A^{ex,hs}[\rho_i(\mathbf{r})] = \int d\mathbf{r}_1 \Phi[n_\alpha(\mathbf{r}_1)] \tag{16}$$

where $\Phi[n_\alpha(\mathbf{r})]$ is given by

$$\Phi[n_\alpha(\mathbf{r})] = -n_0 \ln(1 - n_3) + \frac{n_1 n_2 - \mathbf{n}_{v1}\cdot\mathbf{n}_{v2}}{1 - n_3} + \frac{n_2^3 - 3n_2(\mathbf{n}_{v2}\cdot\mathbf{n}_{v2})}{24\pi(1 - n_3)^2} \tag{17}$$

and $n_\alpha(\alpha = 0,1,2,3, v1, v2)$ are the fundamental measures.

The attraction term $A^{ex,\,att}[\rho_i(\mathbf{r})]$ is accounted for by the mean field approximation[54]

$$\beta A^{ex,att}[\rho_i(\mathbf{r})] = \frac{1}{2}\sum_{i=1}^{m}\sum_{j=1}^{m}\int d\mathbf{r}_1 d\mathbf{r}_2 \beta u_{ij}^{att}(|\mathbf{r}_2 - \mathbf{r}_1|) \rho_i(\mathbf{r}_1)\rho_j(\mathbf{r}_2) \tag{18}$$

Wertheim's TPT1,[37−40] as extended by Chapman,[55] is used to calculate $A^{ex,\,assoc}[\rho_i(\mathbf{r})]$ and $A^{ex,\,chain}[\rho_i(\mathbf{r})]$. The association free energy functional is

$$\beta A^{ex,assoc}[\rho_i(\mathbf{r})] = \int d\mathbf{r}_1 \sum_{i=1}^{m} \rho_i(\mathbf{r}_1) \times \sum_{\alpha\in\Gamma^{(i)}} \left(\ln \chi_\alpha^i(\mathbf{r}_1) - \frac{\chi_\alpha^i(\mathbf{r}_1)}{2} + \frac{1}{2}\right) \tag{19}$$

The first summation is over all segments *i* and the second is over all the association sites on segment *i*. χ_α^i denotes the fraction of segments of type *i* that are not bonded at their

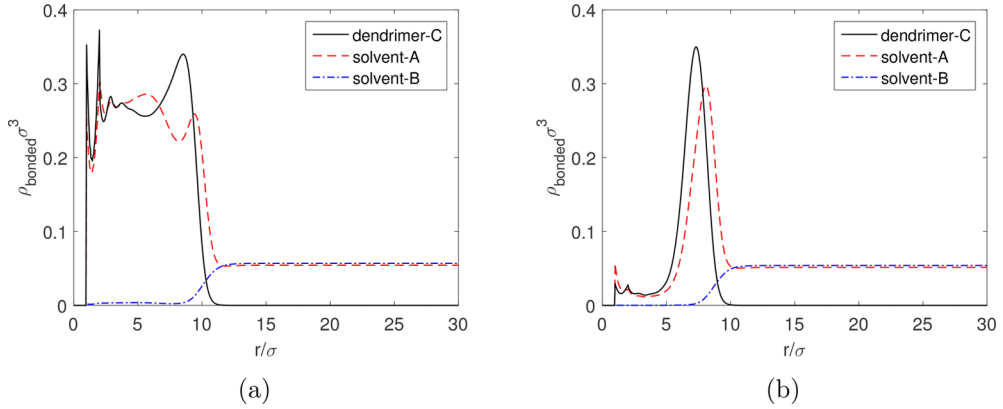

Figure 11. (a) Density profiles of bonded dendrimer and solvent sites at $T = 275$ K. (b) Density profiles of bonded dendrimer and solvent sites at $T = 280$ K. $\varepsilon^{LJ}_{DD}/k_b = \varepsilon^{LJ}_{SS}/k_b = 250$ K, $\varepsilon^{LJ}_{DS}/k_b = 0$, $\varepsilon^{assoc}_{AC}/k_b = 2700$ K, $\varepsilon^{assoc}_{AB}/k_b = 1000$ K, and $\rho_S\sigma^3 = 0.6$ at bulk.

DOI: 10.1021/acs.langmuir.9b00514
Langmuir 2019, 35, 10808−10817

associating site α, which can be obtained by the law of mass action[55,56]

$$\chi_\alpha^i(\mathbf{r}_1) = \frac{1}{1 + \int d\mathbf{r}_2 \sum_{j=1}^{m} \rho_j(\mathbf{r}_2) \times \sum_{\beta \in \Gamma^{(j)}} \chi_\beta^j(\mathbf{r}_2) \Delta^{ij}(\mathbf{r}_1, \mathbf{r}_2)} \tag{20}$$

The association strength $\Delta^{ij}(\mathbf{r}_1, \mathbf{r}_2)$ is controlled by

$$\Delta^{ij}(\mathbf{r}_1, \mathbf{r}_2) = KF^{ij}(\mathbf{r}_1, \mathbf{r}_2) y^{ij}(\mathbf{r}_1, \mathbf{r}_2) \tag{21}$$

where K is a constant geometric factor, which accounts for the entropic cost associated with the orientations and bonding volume of two segments. $F^{ij}(\mathbf{r}_1, \mathbf{r}_2)$ is the associating Mayer-f function given as[41]

$$F^{ij}(\mathbf{r}_1, \mathbf{r}_2) = \exp[\beta\varepsilon_0 - \beta v_{\text{bond}}^{ij}(\mathbf{r}_1, \mathbf{r}_2)] - 1 \tag{22}$$

where ε_0 is the bond energy and $v_{\text{bond}}^{ij}(\mathbf{r}_1, \mathbf{r}_2)$ is the bonding potential. In the complete association limit of $\varepsilon_0 \to \infty$, the chain contribution to the free energy $A^{\text{ex, chain}}[\rho_i(\mathbf{r})]$ can be obtained. For tangentially bonded segments, the bonding potential is given by

$$\exp[-\beta v_{\text{bond}}^{ij}(\mathbf{r}_1, \mathbf{r}_2)] = \frac{\delta(|\mathbf{r}_1 - \mathbf{r}_2| - \sigma^{ij})}{4\pi(\sigma^{ij})^2} \tag{23}$$

and $y^{ij}(\mathbf{r}_1, \mathbf{r}_2)$ is the cavity correlation function for inhomogeneous hard sphere reference fluid. $y^{ij}(\mathbf{r}_1, \mathbf{r}_2)$ is approximated by[41]

$$\ln y^{ij}(\mathbf{r}_1, \mathbf{r}_2) = \frac{1}{2}\{\ln y^{ij}[\bar{\rho}_k(\mathbf{r}_1)] + \ln y^{ij}[\bar{\rho}_k(\mathbf{r}_2)]\} \tag{24}$$

where $\bar{\rho}_k(\mathbf{r}_1)$ is the weighted density of segment k at position $\mathbf{r}_1$. In the current work, a simple weighting is used

$$\bar{\rho}_k(\mathbf{r}_1) = \frac{3}{4\pi(\sigma_k)^3} \int_{|\mathbf{r}_1 - \mathbf{r}_2| < \sigma_k} d\mathbf{r}_2 \rho_k(\mathbf{r}_2) \tag{25}$$

and the expression for $y^{ij}[\bar{\rho}_k(\mathbf{r}_1)]$, the cavity correlation function for homogeneous hard sphere fluid, is only needed at contact and can be found in the work of Tripathi and Chapman.[34]

Further details and applications of the theory can be found in previous works.[31,36,41,42,56−61]

AUTHOR INFORMATION

Corresponding Author

*E-mail: wgchap@rice.edu.

ORCID

Yuchong Zhang: 0000-0002-6809-1020

Walter G. Chapman: 0000-0002-8789-9041

Notes

The authors declare no competing financial interest.

ACKNOWLEDGMENTS

We thank the Robert A. Welch Foundation (grant no. C-1241) for financial support.

REFERENCES

(1) Roy, D.; Brooks, W. L.; Sumerlin, B. S. New directions in thermoresponsive polymers. *Chem. Soc. Rev.* **2013**, *42*, 7214−7243.

(2) Ward, M. A.; Georgiou, T. K. Thermoresponsive polymers for biomedical applications. *Polymers* **2011**, *3*, 1215−1242.

(3) Schild, H. G. Poly (N-isopropylacrylamide): experiment, theory and application. *Prog. Polym. Sci.* **1992**, *17*, 163−249.

(4) Haba, Y.; Harada, A.; Takagishi, T.; Kono, K. Rendering poly (amidoamine) or poly (propylenimine) dendrimers temperature sensitive. *J. Am. Chem. Soc.* **2004**, *126*, 12760−12761.

(5) Tono, Y.; Kojima, C.; Haba, Y.; Takahashi, T.; Harada, A.; Yagi, S.; Kono, K. Thermosensitive properties of poly (amidoamine) dendrimers with peripheral phenylalanine residues. *Langmuir* **2006**, *22*, 4920−4922.

(6) Jia, Z.; Chen, H.; Zhu, X.; Yan, D. Backbone-thermoresponsive hyperbranched polyethers. *J. Am. Chem. Soc.* **2006**, *128*, 8144−8145.

(7) Haba, Y.; Kojima, C.; Harada, A.; Kono, K. Comparison of thermosensitive properties of Poly (amidoamine) dendrimers with Peripheral N-Isopropylamide groups and linear polymers with the same groups. *Angew. Chem., Int. Ed.* **2007**, *119*, 238−241.

(8) Liu, H.; Chen, Y.; Shen, Z. Thermoresponsive hyperbranched polyethylenimines with isobutyramide functional groups. *J. Polym. Sci., Part A: Polym. Chem.* **2007**, *45*, 1177−1184.

(9) Chen, H.; Jia, Z.; Yan, D.; Zhu, X. Thermo-Responsive Highly Branched Polyethers by Proton-Transfer Polymerization of 1, 2, 7, 8-Diepoxyoctane and Multiols. *Macromol. Chem. Phys.* **2007**, *208*, 1637−1645.

(10) Li, W.; Zhang, A.; Feldman, K.; Walde, P.; Schluter, A. D. Thermoresponsive dendronized polymers. *Macromolecules* **2008**, *41*, 3659−3667.

(11) Liu, X.-Y.; Mu, X.-R.; Liu, Y.; Liu, H.-J.; Chen, Y.; Cheng, F.; Jiang, S.-C. Hyperbranched polymers with thermoresponsive property highly sensitive to ions. *Langmuir* **2012**, *28*, 4867−4876.

(12) Liu, Y.; Liu, X. Y.; Liu, H.-J.; Cheng, F.; Chen, Y. Synthesis of thermoresponsive hyperbranched polyamidoamine and the molecular weight, pH, and anion sensitive thermoresponsive properties thereof. *Macromol. Res.* **2012**, *20*, 578−584.

(13) Aathimanikandan, S. V.; Savariar, E. N.; Thayumanavan, S. Temperature-sensitive dendritic micelles. *J. Am. Chem. Soc.* **2005**, *127*, 14922−14929.

(14) Parrott, M. C.; Marchington, E. B.; Valliant, J. F.; Adronov, A. Synthesis and properties of carborane-functionalized aliphatic polyester dendrimers. *J. Am. Chem. Soc.* **2005**, *127*, 12081−12089.

(15) Xu, J.; Luo, S.; Shi, W.; Liu, S. Two-stage collapse of unimolecular micelles with double thermoresponsive coronas. *Langmuir* **2006**, *22*, 989−997.

(16) Hong, H.; Mai, Y.; Zhou, Y.; Yan, D.; Chen, Y. Synthesis and supramolecular selfassembly of thermosensitive amphiphilic star copolymers based on a hyperbranched polyether core. *J. Polym. Sci., Part A: Polym. Chem.* **2008**, *46*, 668−681.

(17) Kimura, M.; Kato, M.; Muto, T.; Hanabusa, K.; Shirai, H. Temperature-sensitive dendritic hosts: synthesis, characterization, and control of catalytic activity. *Macromolecules* **2000**, *33*, 1117−1119.

(18) Cheng, H.; Xie, S.; Zhou, Y.; Huang, W.; Yan, D.; Yang, J.; Ji, B. Effect of degree of branching on the thermoresponsive phase transition behaviors of hyperbranched multiarm copolymers: comparison of systems with lcst transition based on coil-to-globule transition or hydrophilic- hydrophobic balance. *J. Phys. Chem. B* **2010**, *114*, 6291−6299.

(19) Seidi, F.; Heshmati, P. Synthesis of a PEG-PNIPAm Thermosensitive dendritic copolymer and investigation of its self-association. *Chin. J. Polym. Sci.* **2015**, *33*, 192−202.

(20) Li, X.; Haba, Y.; Ochi, K.; Yuba, E.; Harada, A.; Kono, K. PAMAM dendrimers with an oxyethylene unit-enriched surface as biocompatible temperature-sensitive dendrimers. *Bioconjugate Chem.* **2013**, *24*, 282−290.

(21) Wang, H.; Huang, Q.; Chang, H.; Xiao, J.; Cheng, Y. Stimuli-responsive dendrimers in drug delivery. *Biomater. Sci.* **2016**, *4*, 375−390.

(22) Murat, M.; Grest, G. S. Molecular dynamics study of dendrimer molecules in solvents of varying quality. *Macromolecules* **1996**, *29*, 1278−1285.

(23) Giupponi, G.; Buzza, D. Monte Carlo simulation of dendrimers in variable solvent quality. *J. Chem. Phys.* **2004**, *120*, 10290−10298.

DOI: 10.1021/acs.langmuir.9b00514
Langmuir 2019, 35, 10808−10817

(24) Ballauff, M.; Likos, C. N. Dendrimers in solution: insight from theory and simulation. *Angew. Chem., Int. Ed.* **2004**, *43*, 2998−3020.
(25) Markelov, D. A.; Polotsky, A. A.; Birshtein, T. M. Formation of a Hollow interior in the fourth-generation dendrimer with attached oligomeric terminal segments. *J. Phys. Chem. B* **2014**, *118*, 14961−14971.
(26) Wengenmayr, M.; Dockhorn, R.; Sommer, J.-U. Multicore Unimolecular Structure Formation in Single Dendritic−Linear Copolymers under Selective Solvent Conditions. *Macromolecules* **2016**, *49*, 9215−9227.
(27) Chen, C.; Tang, P.; Qiu, F.; Shi, A.-C. Density functional study for homodendrimers and amphiphilic dendrimers. *J. Phys. Chem. B* **2016**, *120*, 5553−5563.
(28) Mendez, S.; Curro, J. G.; McCoy, J. D.; Lopez, G. P. Computational modeling of the temperature-induced structural changes of tethered poly (N-isopropylacrylamide) with self-consistent field theory. *Macromolecules* **2005**, *38*, 174−181.
(29) Lee, S. G.; Pascal, T. A.; Koh, W.; Brunello, G. F.; Goddard, W. A., III; Jang, S. S. Deswelling mechanisms of surface-grafted poly (NIPAAm) brush: Molecular dynamics simulation approach. *J. Phys. Chem. C* **2012**, *116*, 15974−15985.
(30) Lian, C.; Wang, L.; Chen, X.; Han, X.; Zhao, S.; Liu, H.; Hu, Y. Modeling swelling behavior of thermoresponsive polymer brush with lattice density functional theory. *Langmuir* **2014**, *30*, 4040−4048.
(31) Gong, K.; Marshall, B. D.; Chapman, W. G. Modeling lower critical solution temperature behavior of associating polymer brushes with classical density functional theory. *J. Chem. Phys.* **2013**, *139*, No. 094904.
(32) Zhang, Y.; Valiya Parambathu, A.; Chapman, W. G. Density functional study of dendrimer molecules in solvents of varying quality. *J. Chem. Phys.* **2018**, *149*, No. 064904.
(33) Evans, R. Density functionals in the theory of nonuniform fluids. *Fundam. Inhomogeneous Fluids* **1992**, *1*, 85−176.
(34) Tripathi, S.; Chapman, W. G. Microstructure of inhomogeneous polyatomic mixtures from a density functional formalism for atomic mixtures. *J. Chem. Phys.* **2005**, *122*, No. 094506.
(35) Wu, J. Density functional theory for chemical engineering: From capillarity to soft materials. *AIChE J.* **2006**, *52*, 1169−1193.
(36) Emborsky, C. P.; Feng, Z.; Cox, K. R.; Chapman, W. G. Recent advances in classical density functional theory for associating and polyatomic molecules. *Fluid Phase Equilib.* **2011**, *306*, 15−30.
(37) Wertheim, M. S. Fluids with highly directional attractive forces. I. Statistical thermodynamics. *J. Stat. Phys.* **1984**, *35*, 19−34.
(38) Wertheim, M. S. Fluids with highly directional attractive forces. II. Thermodynamic perturbation theory and integral equations. *J. Stat. Phys.* **1984**, *35*, 35−47.
(39) Wertheim, M. S. Fluids with highly directional attractive forces. III. Multiple attraction sites. *J. Stat. Phys.* **1986**, *42*, 459−476.
(40) Wertheim, M. S. Fluids with highly directional attractive forces. IV. Equilibrium polymerization. *J. Stat. Phys.* **1986**, *42*, 477−492.
(41) Jain, S.; Dominik, A.; Chapman, W. G. Modified interfacial statistical associating fluid theory: A perturbation density functional theory for inhomogeneous complex fluids. *J. Chem. Phys.* **2007**, *127*, 244904.
(42) Bymaster, A.; Chapman, W. G. Ani-SAFT density functional theory for associating polyatomic molecules. *J. Phys. Chem. B* **2010**, *114*, 12298−12307.
(43) Chandler, D.; Weeks, J. D. Equilibrium structure of simple liquids. *Phys. Rev. Lett.* **1970**, *25*, 149.
(44) Weeks, J. D.; Chandler, D.; Andersen, H. C. Role of repulsive forces in determining the equilibrium structure of simple liquids. *J. Chem. Phys.* **1971**, *54*, 5237−5247.
(45) Chai, M.; Niu, Y.; Youngs, W. J.; Rinaldi, P. L. Structure and conformation of DAB dendrimers in solution via multidimensional NMR techniques. *J. Am. Chem. Soc.* **2001**, *123*, 4670−4678.
(46) Prosa, T. J.; Bauer, B. J.; Amis, E. J.; Tomalia, D. A.; Scherrenberg, R. A SAXS study of the internal structure of dendritic polymer systems. *J. Polym. Sci., Part B: Polym. Phys.* **1997**, *35*, 2913−2924.
(47) Rosenfeldt, S.; Dingenouts, N.; Ballauff, M.; Werner, N.; Vögtle, F.; Lindner, P. Distribution of end groups within a dendritic structure: a SANS study including contrast variation. *Macromolecules* **2002**, *35*, 8098−8105.
(48) Djeda, R.; Ruiz, J.; Astruc, D.; Satapathy, R.; Dash, B. P.; Hosmane, N. S. Click Synthesis and Properties of Carborane-Appended Large Dendrimers. *Inorg. Chem.* **2010**, *49*, 10702−10709.
(49) Wang, Y.; Grayson, S. M. Approaches for the preparation of non-linear amphiphilic polymers and their applications to drug delivery. *Adv. Drug Delivery Rev.* **2012**, *64*, 852−865.
(50) You, Y.-Z.; Hong, C.-Y.; Pan, C.-Y.; Wang, P.-H. Synthesis of a Dendritic Core−Shell Nanostructure with a Temperature-Sensitive Shell. *Adv. Mater.* **2004**, *16*, 1953−1957.
(51) Zhuang, J.; Gordon, M. R.; Ventura, J.; Li, L.; Thayumanavan, S. Multi-stimuli responsive macromolecules and their assemblies. *Chem. Soc. Rev.* **2013**, *42*, 7421−7435.
(52) Parrott, M. C.; Valliant, J. F.; Adronov, A. Thermally induced phase transition of carborane-functionalized aliphatic polyester dendrimers in aqueous media. *Langmuir* **2006**, *22*, 5251−5255.
(53) Rosenfeld, Y. Free-energy model for the inhomogeneous hard-sphere fluid mixture and density-functional theory of freezing. *Phys. Rev. Lett.* **1989**, *63*, 980.
(54) Hansen, J.-P.; McDonald, I. R. *Theory of simple liquids*; Elsevier, 1990.
(55) Chapman, W. G. *Theory and simulation of associating liquid mixtures*. Ph.D. thesis, Cornell University, 1988.
(56) Segura, B. C. J.; Shukla, W. G. C. A. K. P. Associating fluids with four bonding sites against a hard wall: density functional theory. *Mol. Phys.* **2010**, *90*, 759−772.
(57) Jain, S.; Jog, P.; Weinhold, J.; Srivastava, R.; Chapman, W. G. Modified interfacial statistical associating fluid theory: Application to tethered polymer chains. *J. Chem. Phys.* **2008**, *128*, 154910.
(58) Gong, K.; Chapman, W. G. Solvent response of mixed polymer brushes. *J. Chem. Phys.* **2011**, *135*, 214901.
(59) Gong, K.; Marshall, B. D.; Chapman, W. G. Response behavior of diblock copolymer brushes in explicit solvent. *J. Chem. Phys.* **2012**, *137*, 154904.
(60) Xi, S.; Wang, L.; Liu, J.; Chapman, W. Thermodynamics, Microstructures, and Solubilization of Block Copolymer Micelles by Density Functional Theory. *Langmuir* **2019**, *35*, 5081.
(61) Liu, J.; Xi, S.; Chapman, W. G. Competitive Sorption of CO_2 with Gas Mixtures in Nanoporous Shale for Enhanced Gas Recovery from Density Functional Theory. *Langmuir* **2019**, *35*, 8144.

DOI: 10.1021/acs.langmuir.9b00514
Langmuir 2019, 35, 10808−10817